tvst

Article

Identification of Subclinical Microvascular Biomarkers in Coronary Heart Disease in Retinal Imaging

Julia Aschauer[1,2,*], Stefan Aschauer[3,*], Andreas Pollreisz[1,2], Felix Datlinger[1,2], Constantin Gatterer[3], Georgios Mylonas[1], Berit Egner[1], Dominik Hofer[1], Irene Steiner[4], Christian Hengstenberg[3], and Ursula Schmidt-Erfurth[1]

[1] Department of Ophthalmology and Optometry, Medical University of Vienna, Vienna, Austria
[2] Vienna Clinical Trial Center, Medical University of Vienna, Vienna, Austria
[3] Division of Cardiology, Department of Internal Medicine II, Medical University of Vienna, Vienna, Austria
[4] CeMSIIS, Institute for Medical Statistics, Medical University of Vienna, Vienna, Austria

Purpose: Cardiovascular disease and foremost coronary heart disease (CHD) are the worldwide leading causes of death. The aim of this study was to use non-invasive, multi-model retinal imaging to define microvascular features in patients with and without coronary angiography (CA)-confirmed CHD.

Methods: In this prospective, cross-sectional pilot study we included adult patients who presented to a tertiary referral center for elective CA due to suspected CHD. All patients underwent widefield fundus photography for retinopathy grading. Optical coherence tomography angiography was used to measure vessel density (VD) of the individual capillary plexuses in 6 × 6-mm macular volume scans. Adaptive optics imaging was performed to assess the first-order arteriolar lumen diameter (LD), total diameter (TD), wall-to-lumen ratio (WLR), and wall cross-section area, as well as to qualitatively describe vessel morphology.

Results: Of the included 45 patients (13 females; 65 ± 10 years old), 27 were confirmed with CHD in elective CA. The most prevalent retinal vascular pathologies were arteri-ovenous nickings, focal arterial narrowings, and microaneurysms. VD in the superficial capillary plexus, deep capillary plexus, and choriocapillaris was lower in CHD patients, although the odds ratios were not significantly different from 1 ($P = 0.06$–0.92). Median arterial LD, TD, and WLR values were 98.3 µm (interquartile range [IQR] = 13.0), 122.9 µm (IQR = 17.6), and 0.26 µm (IQR = 0.07), respectively, with a trend toward a higher WLR in CHD patients.

Conclusions: In a cardiovascular risk population, high-resolution quantitative and qualitative microvascular phenotyping in the retina may provide valuable subclinical indicators for coronary artery impairment, although larger clinical trials are needed.

Translational Relevance: Subclinical retinal microvascular changes may serve as non-invasive, cost-effective biomarkers for risk stratification of patients with CHD.

Introduction

Cardiovascular disease (CVD) is the worldwide leading cause of death. The World Health Organization has estimated that 17.9 million people died from CVD in 2016, accounting for 31% of all global deaths. The two major forms of CVD are coronary heart disease (CHD) and stroke, which are responsible for 85% of CVD deaths. The current gold standard in the diagnosis of CHD is coronary microvasculature assessment using invasive coronary angiography (CA), even though the diagnosis of significant CHD cannot be confirmed during the procedure in about 40% of all patients undergoing CA.[1] In contrast, other patients may not present to their cardiologists until late in

translational vision science & technology

symptom development and are just being referred at the time when complications of the disease, such as myocardial infarction, have already occurred. Therefore, an efficient population-based screening tool and risk assessment are required in order to detect signs of CHD (and CVD) at an early, asymptomatic, and possibly "subclinical" stage and to initiate preventive actions and a stratified monitoring, as well as timely therapy, in the individual patient. The currently available CVD risk prediction tools are limited to a low number of well-established risk factors that show a linear correlation with CVD risk.[2,3] However, these algorithms are unable to reflect the response to treatment and are associated with restricted modeling assumptions.[4]

The delicate microvasculature of the coronary vascular tree shares common physiologic and anatomic characteristics with the retinal microvasculature.[5] However, in contrast to the coronary vascular system, the microvascular architecture and perfusion of the retina can be visualized non-invasively to study the actual microvascular architecture of affected patients in vivo. Hence, integration of retinal non-invasive, quantitative, and qualitative microvascular phenotyping may enhance the performance of cardiovascular risk assessment tools in the future.

Major technological advances in ophthalmology have led to the introduction of retinal optical coherence tomography angiography (OCTA), which allows far more expedient microvascular retinal imaging. OCTA analyzes the variance in light speckle produced by erythrocyte flow and thereby generates a contrast-free retinal angiogram of the individual interconnected retinal capillary plexuses with unparalleled accuracy in micrometer resolution. Lower vessel density in the superficial capillary plexus has already been shown to be associated with impaired left ventricular function and increased cardiovascular risk in a small pilot study of patients with acute coronary syndrome,[6] as well as with the occurrence of acute kidney injury with iodinated contrast agent after CA in patients at high cardiovascular risk.[7]

In addition to OCTA, adaptive optics (AO) fundus imaging is another novel approach for non-invasively assessing the qualitative features of the retinal microcirculation; AO allows quantitative measurement of the retinal vessel geometry at a near-histologic scale. This technique has been applied to study microcirculatory changes in patients with diabetes mellitus,[8] as well as hypertension,[9] and results point to a correlation between increased arterial wall-to-lumen ratio (WLR) with a higher mean blood pressure and older age.[10] Moreover, WLR was proposed as a sensitive marker of short- and long-term blood pressure changes.[9]

Subclinical retinal microvascular changes thus may serve as precious non-invasive and cost-effective biomarkers in the evaluation of patients with CVD, and especially CHD, but their incremental value in risk stratification still remains to be explored. The aims of the present prospective pilot study were to qualitatively and quantitatively describe microvascular features obtained from a non-invasive, multimodel retinal imaging approach in patients with manifest risk of CVD, with and without significant CHD.

Methods

Our study was a prospective, cross-sectional, single-center pilot study conducted at the Department of Ophthalmology and Optometry and the Department of Internal Medicine II, Division of Cardiology, of the Medical University of Vienna. All study investigations complied with the tenets of the Declaration of Helsinki. The study was approved by the Ethics Committee of the Medical University of Vienna (EK1935/2019), and written informed consent was obtained from all patients prior to study inclusion.

We included consecutive adult patients who presented to the tertiary referral center of the Department of Internal Medicine II, Division of Cardiology, for suspected CHD and who were scheduled for elective CA intervention. Defined exclusion criteria were the funduscopic presence of ocular diseases (e.g., age-related macular degeneration, uncontrolled glaucoma, retinal vascular occlusion), media opacities (cataract, vitreous hemorrhage), and intraocular inflammation, as well as a history of previous laser or intraocular surgery or intravitreal medication. Furthermore, patients with diabetes mellitus were excluded in order to rule out the presence of (subclinical) signs of diabetic retinopathy.

Clinical Evaluation for Cardiovascular Disease

Patients were recruited at the outpatient clinic of the Division of Cardiology, where all patients received a physical examination, a thorough medical history (including their current medication, smoking status, history of hypertension/hyperlipidemia, stroke, and myocardial infarction), and routine blood samplings, including HbA1c, total cholesterol, lipoprotein(a), and creatinine. Invasive CA was performed via radial or femoral artery access with standard practices and projections using an iso-osmolar contrast agent (iodixanol, VISIPAQUE 320; GE Healthcare, Chicago,

IL). The examination was monitored by an experienced interventional cardiologist. Intracoronary lumen narrowing of >50% was classified as significant coronary artery stenosis (CAS).

Clinical Evaluation at the Department of Ophthalmology

After Snellen best-corrected visual acuity testing, examination of the anterior segment, intraocular pressure measurement, and axial eye length measurement with laser biometry, all patients underwent AO retinal fundus imaging in miosis prior to pupil dilatation by installing eye drops (0.5% tropicamide, Mydriaticum; AGEPHA Pharma, Senec, Slovakia). Retinal imaging in mydriasis included widefield fundus photography and OCTA, which were followed by a dilated fundus biomicroscopy by a retina specialist.

Adaptive Optics Fundus Imaging

The commercially available, flood-illumination RTX1-e Adaptive Optics Retinal Camera (Imagine Optics, Orsay, France) was used to acquire high-resolution en face reflectance images with a field of view of 4° × 4° (equivalent to approximately 1.2 × 1.2 mm in emmetropic eyes) on the retinal fundus. It uses a 850-nm super luminescent diode source and an AO system operating in a closed loop to correct for wavefront aberrations to achieve a resolution of 1.1 µm in the retina.

Gaze was navigated by an internal target in order to capture the reference site in the acquired field: the first temporal arteriolar branch (in order to capture one first order arteriole) of the superior vascular arcade and the first temporal arteriolar bifurcation of inferior vascular arcade, which were at least one disc diameter apart from the optic disc. A live display of the AO-corrected fundus image allowed for adjustment of brightness, contrast, and focus, which were the criteria used for quality control.

After quality assessment, all images were analyzed by the same grader (BE) blinded to the patients' clinical data with the semiautomated AOdetect software (version 003.003.20171026). For each study eye, we performed the analyses at three independent vessel locations of the first-order arteriole in order to output the average results of the three consecutive measurement locations. The automated wall segmentation and thickness computation resulted in the following AO parameters: lumen diameter (LD), total diameter (TD), WLR (= 2 × [wall thickness/lumen diameter]), and wall cross-section area (WCSA; measured on the basis of total vessel diameter and lumen diameter). All analyses were adjusted for the axial length of the study eye. Furthermore, all images were evaluated for qualitative morphologic characteristics including arteriovenous nickings (AVNs), focal arteriolar narrowing (FAN), asymmetric wall thickening, and wall/lumen hyperreflectivity.

Widefield Fundus Photography

Widefield fundus photography was performed using the CLARUS 700 device (software version 1.1.1.45119; Carl Zeiss Meditec, Jena, Germany). With a single capture, the device produces a 90° high-definition widefield image with a resolution of 7.3 µm in the retina. Using the true color mode, one can acquire images that closely resemble the actual coloration of the fundus. After quality control of the images in all study eyes (including brightness, focus, blur, contrast), the same investigator (BE), who was masked for the clinical data of the patient, performed qualitative retinopathy grading in the whole image, as well as in the individual retinal quadrants (superior temporal, inferior temporal, superior nasal, and inferior nasal) considering the presence of the following lesions: blot hemorrhage (H), microaneurysm (MA), pigment clumps (PC), exudates (E), AVNs, FAN, diffuse arteriolar narrowing (DAN), venous beading (VB), venous tortuosity (VT), and cotton wool spots (CWS). Each lesion was graded separately for its number (H, MA, PC, E, AVCs, FAN) or its presence (DAN, VB, VT, CWS). Furthermore, each eye was given a numerical score (0–10). For the presence of each respective lesion, we considered one score point, irrespective of its extent or number.

Optical Coherence Tomography Angiography

OCTA was performed with the PLEX Elite 9000 (Carl Zeiss Meditec) using a swept-source tunable laser with a center wavelength of 1060 nm and a scan speed of 100-kHz A-scans per second to achieve an axial resolution of 6.3 µm and transverse resolution of 20 µm in tissue. We acquired 6 × 6-mm, fovea-centered volume scans. Imaging was repeated until sufficient image quality was achieved in the absence of motion artifacts, misalignment, poor contrast, or uneven illumination. We included only images with a signal strength index score of 8 or higher out of 10. All retinal layers in the corresponding structural B-scans were automatically segmented by the software of the machine (software version PLEX Elite
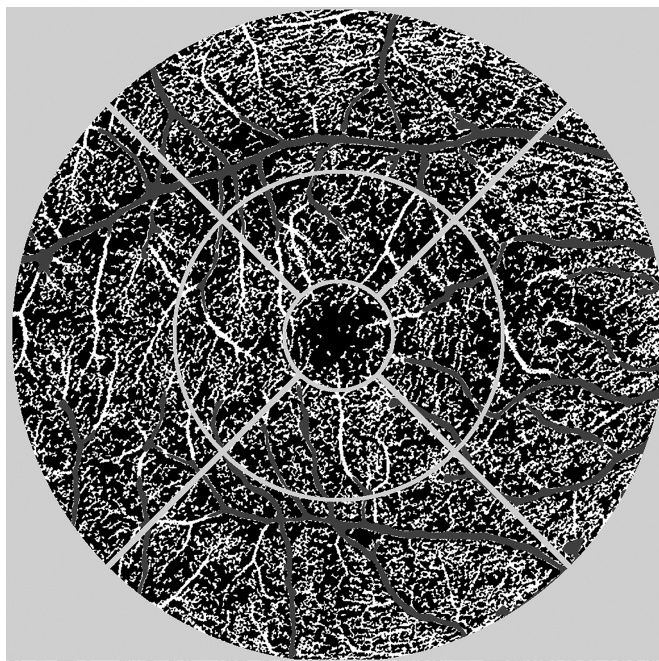
Figure 1. Illustration of the OCTA image analysis algorithm. A nine-field, fovea-centered grid was used as an overlay on the exported images (*light gray*). Using a predefined flow signal threshold, large vessels (*dark gray*) were excluded from the analysis. Perfused vessel density is shown in *white*.

90002.0.147652) followed by manual layer segmentation correction if applicable by the same masked investigator (BE).

En face OCTA images of the superficial capillary plexus (SCP) and deep capillary plexus (DCP), as well as the full retina and the choriocapillaris (CC), were generated and exported for further analysis. Vascular projection artifacts were removed from the DCP using the system settings. Furthermore, the foveal avascular zone (FAZ) was manually traced by the same investigator (BE) using Image J (National Institutes of Health, Bethesda, MD) for FAZ area (μm^2) calculations in the full OCTA volume.

Vessel density (VD), referring to the percentage of vessel area with blood flow over total area measured, was measured in a binary image using a predefined signal flow threshold with exclusion of the larger capillary vessels due to the higher signal intensity of these vessels (Fig. 1) in the SCP, DCP, CC, and the full retina in nine individual sectors corresponding to the 6-mm diameter Early Treatment of Diabetic Retinopathy Study grid centered on the fovea, where segments two to five were united to form the inner ring and segments six to nine to form the outer ring for our further analyses. We hereby used an automated algorithm developed by the Vienna Reading Center at the Medical University of Vienna.

Selection of the Study Eye

Imaging as described was performed in both eyes of a patient following the inclusion/exclusion criteria. Due to imaging difficulties, sufficient image quality could not be achieved for both eyes for all imaging modalities in every patient. Hence, selection of the study eye for all statistical analyses was based on the following criteria: (1) If all imaging modalities passed quality control in both eyes, then one study eye was randomly selected with the sample() function in R (R Foundation for Statistical Computing, Vienna, Austria). (2) If some imaging results did not fulfill quality control criteria in one eye, then we selected the eye with the most examinations with sufficient imaging criteria to be the study eye.

Statistical Analysis

All statistical analyses were performed by a statistician (IS) at the CeMSIIS, Institute for Medical Statistics, Medical University of Vienna, using R 3.6.2. For quantitative variables, we report the mean $\pm$ standard deviation (SD) or median and interquartile range (IQR). For qualitative variables we report the absolute and relative frequencies. For group comparisons (baseline characteristics) of quantitative variables, two-sample *t*-tests for unequal variances were applied if the data were approximately normal distributed; otherwise, Wilcoxon rank-sum tests were calculated. For group comparisons (baseline characteristics) of qualitative variables, χ^2 tests were used or Fisher's exact tests, if the expected frequency was less than 5. Univariate logistic regression models were applied with the status "confirmed significant coronary heart disease, CHD" as the dependent variable to calculate the odds ratio (OR) with its 95% confidence limits and the respective *P* value (OR = 1) for independent predictor variables of the OCTA and AO image results. For all AO fundus camera calculations, the respective axial length was included in the model as an additional independent variable. The significance level was set to 0.05 with a descriptive interpretation of all *P* values due to the exploratory character of the study.

Results

We included 45 patients (13 female) with a high suspicion of coronary heart disease due to cardiovascular symptom presentation diagnosed by a cardiologist in this pilot study. After elective CA intervention, 27 patients (60%) were confirmed to have CHD. The baseline clinical and relevant laboratory

Table 1. Baseline Clinical and Laboratory Characteristics of the Study Population

Characteristic	Total Population (n = 45)	CHD (n = 27)	No CHD (n =18)	P
Female gender, n (%)	13 (29)	6 (22)	7 (39)	0.38
Age (yr), mean (SD)	65 (10)	64 (10)	67 (10)	0.30
Stroke, n (%)	1 (2)	1 (4)	0 (0)	—
Smoker, n (%)	9 (20)	7 (26)	2 (11)	0.49[a]
Former smoker, n (%)	15 (33)	8 (30)	7 (39)	0.49[a]
History of arterial hypertension, n (%)	35 (78)	22 (82)	13 (72)	0.29[a]
Hyperlipidemia, n (%)	30 (67)	19 (70)	11 (61)	0.24[a]
HbA1c (%), mean (SD)	5.5 (0.4)	5.6 (0.5)	5.4 (0.2)	0.013
Total cholesterol (mg/dL), mean (SD)	151 (46)	151 (53)	151 (35)	0.98
Creatinine (mg/dL), mean (SD)	1.0 (0.2)	1.0 (0.2)	0.9 (0.2)	0.19
Lipoprotein(a) (nmol/L), mean (minimum–maximum)	31.5 (7–339)	25 (7–339)	38 (7–218)	0.85[b]

[a]Fisher's exact test.
[b]Wilcoxon rank-sum test.
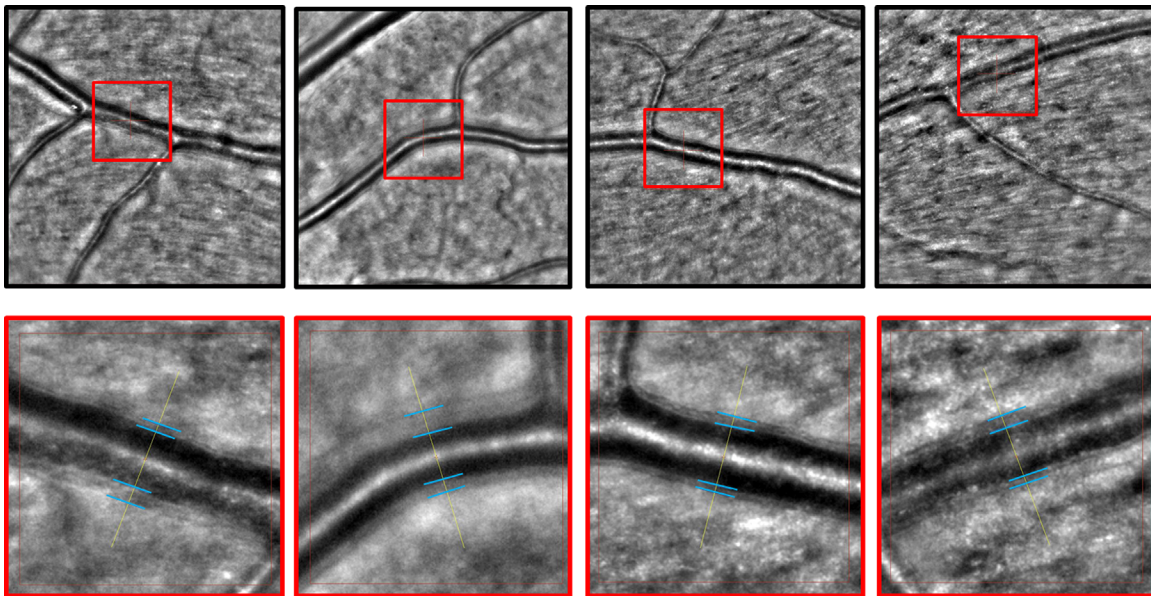
Figure 2. AO fundus camera exemplary images. The *upper row* shows 4° × 4° images of a first-order arteriole with a marked region of interest within a *red square*. The *lower row* shows the magnification of the *red square* from the reference image above with *blue lines* highlighting the vessel wall borders. They show asymmetric vessel wall diameters in this cardiovascular risk population.

characteristics are given in Table 1. Grading of widefield fundus images showed that most of the patients in this population had signs of retinopathy, most likely being AVNs, followed by FAN, MA, VT, VB, E, DAN, CWS, and PC, with the least prevalent being blot hemorrhages. Using our scoring system, we found a median score of 3 (IQR = 2) for the presence of retinopathy in the superior temporal quadrant, 3 (IQR = 1) in the inferior temporal quadrant, 2 (IQR = 1) in the superior nasal quadrant, and 2 (IQR = 2) in the inferior nasal quadrant, which highlights the high frequency of visible retinopathy in the temporal retina.

The median arterial lumen diameter was 98.3 μm (IQR = 13.0), the median arterial total diameter was 122.9 μm (IQR = 17.6), the median WCSA was 4348.5 μm^2 (IQR = 852.25), and the median WLR was 0.26 μm (IQR = 0.07) in the total study population. Using AO technology, we were able to visualize peculiar microscopic vascular wall and lumen details including a high prevalence of asymmetric thickening of the
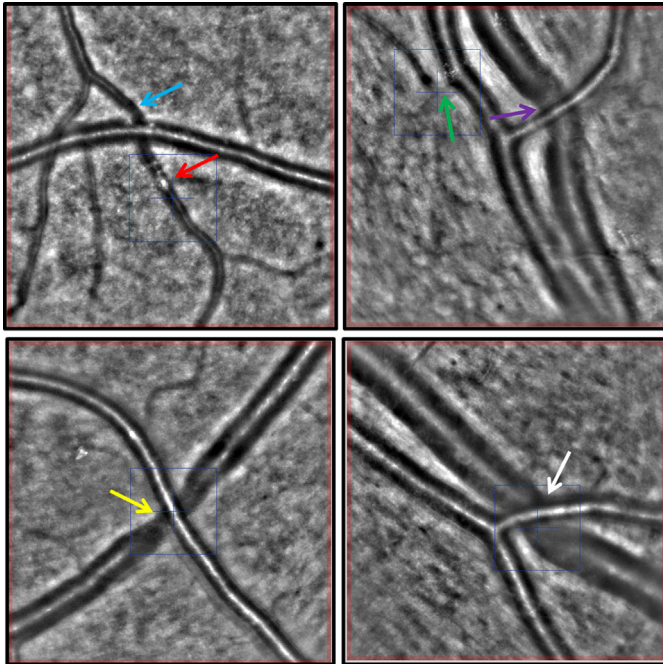
Figure 3. AO fundus camera exemplary images (4° × 4° image sections). The *blue* and *green arrows* mark sites of focal arterial narrowing. The *red arrow* highlights an intraluminal hyperreflective material. The *purple*, *yellow*, and *white arrows* mark sites of AVN at arteriovenous crossing sites.

Table 2. Baseline OCTA Vessel Density Results for the Total Study Population in the Individual Capillary Plexuses and Total Retina

Grid Segment	Total Retina		SCP		DCP		CC	
	Mean	SD	Mean	SD	Mean	SD	Mean	SD
S1	15.5	5.4	16.8	5.3	10.0	5.1	43.0	4.7
S2	3.37	5.4	35.8	4.5	19.6	6.9	37.0	3.0
S3	34.0	5.0	35.7	3.9	18.9	6.4	40.0	2.8
S4	34.2	4.4	36.7	3.7	19.1	6.3	37.7	3.6
S5	34.2	5.2	35.8	4.2	19.2	5.8	39.7	2.5
S6	32.5	3.5	35.6	3.0	16.7	5.7	41.8	2.4
S7	34.0	4.4	35.9	4.2	18.8	5.5	43.0	2.5
S8	33.5	3.5	36.2	2.9	17.7	4.8	42.7	2.3
S9	35.3	4.4	37.8	4.1	18.8	5.6	43.0	2.4
Inner ring	34.0	4.6	36.0	3.8	19.2	6.1	38.6	2.3
Outer ring	33.8	3.0	36.4	2.5	18.0	5.1	42.6	2.0

Segments S1 to S9 are segments one to nine of a grid area centered on the fovea. The inner ring was comprised of segments S2 to S5, and the outer ring was comprised of segments S6 to S9. Values represent vessel density in percent.

arterial vessel walls (Fig. 2), as well as focal arteriolar narrowing, arteriovenous nicking at arteriovenous crossing sites, and the presence of hyperreflective intraluminal material (Fig. 3).

Image quality was high in all patients for OCTA images. The signal strength index was 8/10 in one patient with CHD; all other patients showed a signal strength index of either 9/10 (35% in both groups) or 10/10 (65% in both groups). The FAZ size was 0.22 ± 0.1 in OCTA. The baseline results for VD in the individual nine-field grid areas centered on the fovea for the total retina, as well as the SCP, DCP, and CC individually, are given in Table 2 for the total study population.

Figure 4 illustrates boxplot diagrams for patients with confirmed CHD versus those without confirmed CHD. Vessel density results for the total retina, SCP, DCP, and CC are shown in the upper (inner ring of grid) and middle (outer ring of grid) rows. These boxplots graphically highlight the lower vessel density results in the CHD group throughout the individual plexuses and the total vascular network of the retina. If increasing the OCTA predictor variable (individual capillary plexus vessel densities and FAZ area) by 0.01, the odds of a patient having confirmed significant coronary heart disease in CA decreased, but the odds ratio was not significantly different from 1 (OR, 0.69–0.99; $P = 0.06$–0.92).

The lower row of Figure 4 demonstrates the boxplots for patients with versus without confirmed CHD for the median lumen diameter, total diameter, WCSA, and WLR (from left to right). It shows a smaller median LD but a higher TD and WLR in the CHD group. When the lumen diameter, the total diameter, and the WCSA were increased by 1, the odds of a patient having confirmed CHD decreased for WCSA and increased for the lumen and total diameter, respectively. When the WLR was increased by 0.1, the odds of a patient having CHD decreased. But, all of these odds ratios were not significantly different from 1 (OR, 0.77–1.01; $P = 0.62$–0.76). All of the results of the univariate logistic regression models are illustrated in Table 3.

Discussion

Socioeconomic changes and effects of an aging population have led to an ever-increasing prevalence of CVD as the most threatening chronic disease for human mankind. In the present pilot study, we applied a multimodel, non-invasive imaging approach to describe qualitative and quantitative microvascular retinal features in a small cohort of patients with CVD but with or without confirmed significant CHD. A thorough description of a range of retinal features without an a priori selection seems critical in order to be able to understand the pathophysiologic similarities between these retinal features and coronary microvascular disease and to form the base for future biomarker selection and validation in larger prospective studies.
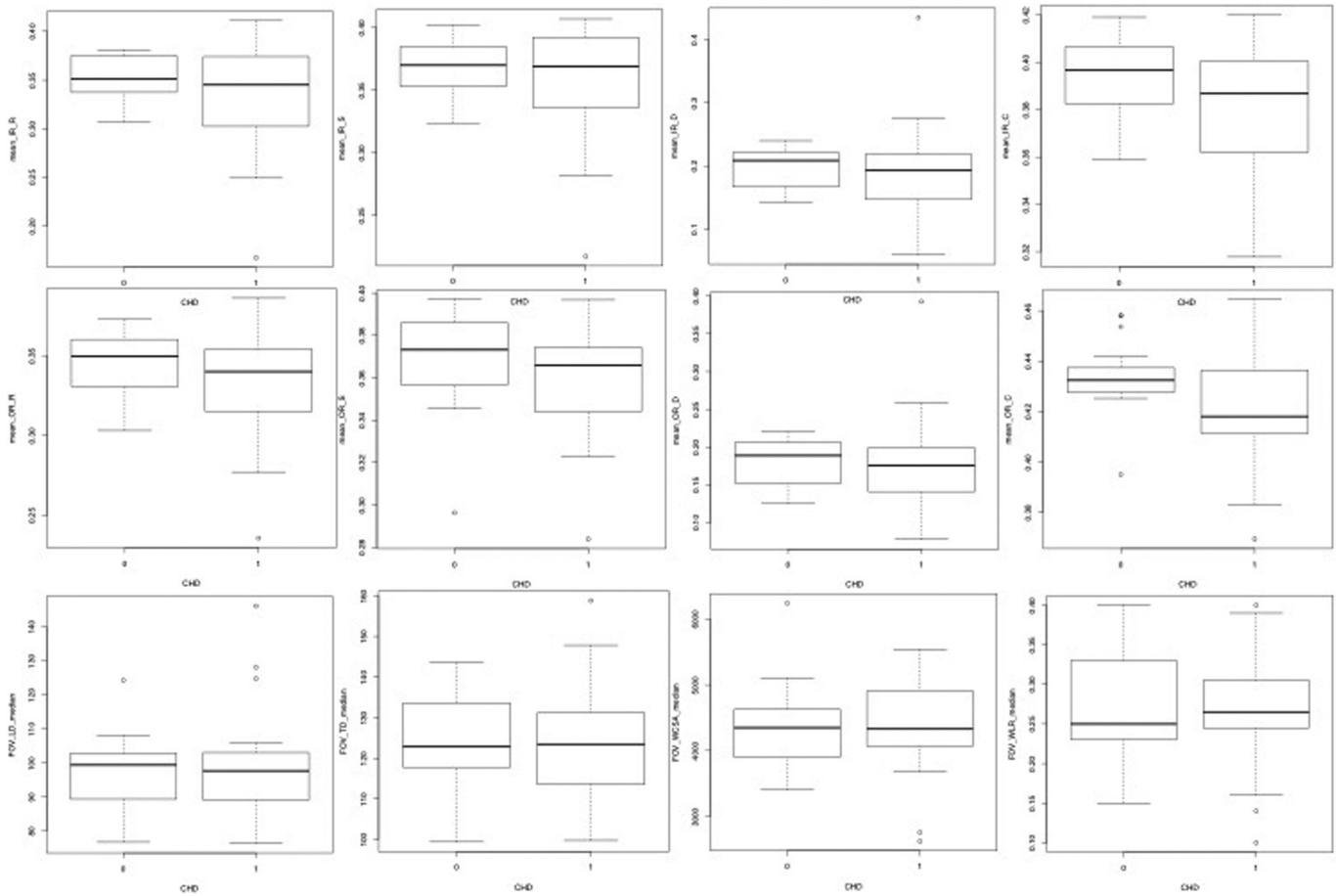
Figure 4.   Boxplots demonstrating differences between patients without (0) and with (1) verified CHD for OCTA inner ring (*upper row*) and outer ring (*middle row*) mean VD results for the total retina (R), superficial/deep capillary plexus (S/D), and choriocapillaris (C), respectively (from *left* to *right*). The *lower row* shows, from *left* to *right*, the median arterial LD, total diameter, wall cross-section area, and WLR differences between the groups.

Population-based studies have shown evidence for an association of retinal vascular caliber, including arteriolar and venular vessel diameters measured from digital fundus photographs, with CHD,[11,12] as well as related cardiovascular risk factors including hypertension,[13] left ventricular remodeling,[14] and aortic distensibility,[15] as well as an increased cardiovascular mortality.[16] However, the results of these studies have thus far not been consistent, and the prognostic meaning of retinal vessel diameters remains controversial. Further, due to limitations in imaging technology at the time, these epidemiologic studies were based only on the assessment of clinically visible microvascular impairment, being qualitative retinopathy grading (i.e., microaneurysms, focal arteriolar narrowing, and hemorrhages) and quantitative computer-assisted measurement of retinal vessel caliber.

Using innovative OCTA imaging, we found a trend of reduced VD in the total retina, as well as the individual retinal (superficial and deep) capillary plexuses and the choriocapillaris layer in patients with significant CHD, as illustrated graphically in Figure 4 and the logistic regression analysis. Even though the results of the model were not statistically significant, which can be explained by the limited study sample size and the fact that all patients had a high risk of CVD in this pilot study, reduced microvascular VD in individual retinal plexuses may serve as a valuable subclinical indicator of the impairment of the coronary vasculature.

There are few prior studies that support our results, with most of them comparing healthy people either with patients with manifest CHD[17] or with patients with acute coronary syndrome, which is a major complication of advanced CHD.[6] These studies have demonstrated reduced vessel densities in retinal[6,17] and choroidal[17] vascular layers in advanced disease stages. In contrast with these studies, we decided to exclude patients with diabetes mellitus, which has been shown to cause subclinical microvascular impairment

Table 3. Univariate Logistic Regression Models for OCTA and AO Fundus Camera Variables Depending on Confirmed CHD

	Estimate	OR	95% LL	95% UL	*P*
OCTA variable					
Retinal inner ring	−0.1029	0.9022	0.754	1.0428	0.2056
Retinal outer ring	−0.1207	0.8863	0.6932	1.094	0.2897
SCP inner ring	−0.1139	0.8924	0.7156	1.0646	0.2507
SCP outer ring	−0.1084	0.8972	0.6718	1.1537	0.4197
DCP inner ring	−0.0184	0.9818	0.8801	1.091	0.7238
DCP outer ring	−0.0066	0.9935	0.8756	1.1303	0.9155
CC inner ring	−0.2511	0.778	0.5523	1.0361	0.1114
CC outer ring	−0.3696	0.691	0.4497	0.9766	0.0565
FAZ area	−0.4124	0.6621	0.3407	1.2157	0.1957
AO variable					
Lumen diameter	0.0115	1.0116	0.963	1.0712	0.6609
Total diameter	0.0088	1.0089	0.954	1.0712	0.759
WCSA	$<−0.1$	0.9998	0.9988	1.0008	0.6931
WLR	−0.265	0.7672	0.2477	2.1749	0.6236

The 95% LL and 95% UL represent the 95% lower and upper limits of the OR, respectively. Axial length was included as an additional independent variable in the model.

including an enlargement/disruption of the FAZ and VD reduction in OCTA.[18,19] Furthermore, results for FAZ area must always be interpreted with caution considering the great variability even in healthy subjects.[20]

We used innovative AO technology to study vessel wall and lumen characteristics of first order arteries in micrometer resolution. As Figure 4 illustrates, the group of patients with significant CHD appears to show smaller median arterial lumen diameters alongside a greater total arterial diameter and WLR; however, this trend is not confirmed in any of the univariate logistic regression models for AO fundus camera data. In addition to the small sample size of the study, this finding may be explained by possible limitations of the AO fundus imaging analysis algorithm. We used the commercially available and manufacturer-recommended semiautomated AOdetect software and performed the analyses at three independent vessel locations of a first-order arteriole in order to output the average results of the three consecutive measurement locations. Still, there remains the possibility of a selection bias when choosing the arterial site for analysis. Future technological advances in these software algorithms may help to further improve the comparability of different study results. Moreover, as arterial hypertension is one of the main risk factors for CVD and CHD, it was not possible to exclude patients with a history of arterial hypertension in this study. Hypertension has been shown to account for about 40% of total WLR variability when combined with the risk factor of age.[10]

On the other hand, high-resolution imaging of retinal arterioles allows precise qualitative microvascular phenotyping, which may be valuable in the management of CVD patients. Figures 2 and 3 demonstrate examples of what we found to be the most prevalent qualitative microvascular features, including asymmetric vessel wall thickening, arteriovenous nicking at crossing sites, and intraluminal hyperreflective material. These changes can currently not be quantitatively compared. Further, it remains to be elucidated whether or not the vascular remodeling in patients with CHD relates to the dual remodeling process of small arteries in patients with hypertension. Here, increased WLR was recently explained to be based either on inward eutrophic remodeling (being a rearrangement of "normal" material along the inner narrowed lumen) or hypertrophic remodeling (which implies hypertrophy and hyperplasia of smooth muscle cells).[21]

The grading of widefield fundus images showed a high prevalence of AVNs, FAN, and MA in this cardiovascular risk population, which has similarly been found by several large population-based studies.[14,16] Interestingly, these clinically manifest lesions were more prominent in the temporal than nasal retinal quadrants, which is consistent with the regional distribution of early retinal lesions in patients with diabetes mellitus.[22,23]

This study was designed as a pilot study, characterized by a small sample size and further, the lack of a control group, as we conducted this study in a cardiovascular risk population, which has to be acknowledged as a major limitation of the study. The precise pathophysiologic mechanisms that contribute to microvascular dysfunction in the retina in patients prone to micro- and macrovascular heart disease remain to be defined. The alterations in microvascular structure and function may at least partly be explained by endothelial dysfunction and the creation of an inflammatory milieu with downstream effects on systemic vascular resistance and tissue perfusion. Moreover, not only has retinal vascular atherosclerosis been shown to strongly correlate with atherosclerosis of the vascular tree expressed by the Gensini score,[24] but also the atherosclerotic changes in retinal arterioles are characterized by wall thickening and lipid deposition in the endothelium–intima and may even demonstrate fibrosis and calcification, resembling the pathologic sequelae of systemic atherosclerosis.[25]

In conclusion, the results of this study suggest that non-invasive, high-resolution imaging of the retinal vascular compartment may offer precious insights into the systemic manifestations of micro- and macrovascular disease. More extensive, larger longitudinal studies are necessary (1) to identify which of the retinal capillary beds are most affected by vessel density rarefication, (2) to define repeatable and standardized AO features that are comparable over different study populations, and (3) to evaluate the integration of the most promising retinal biomarkers in currently available risk-assessment tools augmented by innovative deep-learning algorithms to offer a further step toward the goal of obtaining efficient precision medicine in cardiovascular disease.

Acknowledgments

References

1. Albus C, Barkhausen J, Fleck E, Haasenritter J, Lindner O, Silber S. The diagnosis of chronic coronary heart disease. *Dtsch Arztebl Int*. 2017;114(42):712–719, https://doi.org/10.3238/arztebl.2017.0712.

2. Piepoli MF, Hoes AW, Agewall S, et al. 2016 European Guidelines on cardiovascular disease prevention in clinical practice: the Sixth Joint Task Force of the European Society of Cardiology and Other Societies on Cardiovascular Disease Prevention in Clinical Practice (constituted by representatives of 10 societies and by invited experts) developed with the special contribution of the European Association for Cardiovascular Prevention & Rehabilitation (EACPR). *Atherosclerosis*. 2016;252:207–274, https://doi.org/10.1016/j.atherosclerosis.2016.05.037.

3. Alaa AM, Bolton T, Di Angelantonio E, Rudd JHF, van der Schaar M. Cardiovascular disease risk prediction using automated machine learning: a prospective study of 423,604 UK Biobank participants. *PLoS One*. 2019;14(5):e0213653, https://doi.org/10.1371/journal.pone.0213653.

4. Damen JA, Hooft L, Schuit E, et al. Prediction models for cardiovascular disease risk in the general population: systematic review. *BMJ*. 2016;353:i2416, https://doi.org/10.1136/bmj.i2416.

5. Hughes S, Yang H, Chan-Ling T. Vascularization of the human fetal retina: roles of vasculogenesis and angiogenesis. *Invest Ophthalmol Vis Sci*. 2000;41(5):1217–1228.

6. Arnould L, Guenancia C, Azemar A, et al. The EYE-MI pilot study: a prospective acute coronary syndrome cohort evaluated with retinal optical coherence tomography angiography. *Invest Ophthalmol Vis Sci*. 2018;59(10):4299–4306, https://doi.org/10.1167/iovs.18-24090.

7. Alan G, Guenancia C, Arnould L, et al. Retinal vascular density as a novel biomarker of acute renal injury after acute coronary syndrome. *Sci Rep*. 2019;9(1):8060, https://doi.org/10.1038/s41598-019-44647-9.

8. Lombardo M, Parravano M, Serrao S, Ducoli P, Stirpe M, Lombardo G. Analysis of retinal capillaries in patients with type 1 diabetes and nonproliferative diabetic retinopathy using adaptive optics imaging. *Retina*. 2013;33(8):1630–1639, https://doi.org/10.1097/IAE.0b013e3182899326.

9. Rosenbaum D, Mattina A, Koch E, et al. Effects of age, blood pressure and anti-hypertensive treatments on retinal arterioles remodeling assessed by adaptive optics. *J Hypertens*. 2016;34(6):1115–1122, https://doi.org/10.1097/HJH.0000000000000894.

10. Koch E, Rosenbaum D, Brolly A, et al. Morphometric analysis of small arteries in the human

retina using adaptive optics imaging: relationship with blood pressure and focal vascular changes. *J Hypertens*. 2014;32(4):890–898, https://doi.org/10.1097/HJH.0000000000000095.

11. Wong TY, Klein R, Sharrett AR, et al. Retinal arteriolar narrowing and risk of coronary heart disease in men and women. The Atherosclerosis Risk in Communities Study. *JAMA*. 2002;287(9):1153–1159, https://doi.org/10.1001/jama.287.9.1153.

12. McGeechan K, Liew G, Macaskill P, et al. Risk prediction of coronary heart disease based on retinal vascular caliber (from the Atherosclerosis Risk In Communities [ARIC] Study). *Am J Cardiol*. 2008;102(1):58–63, https://doi.org/10.1016/j.amjcard.2008.02.094.

13. Ding J, Wai KL, McGeechan K, et al. Retinal vascular caliber and the development of hypertension: a meta-analysis of individual participant data. *J Hypertens*. 2014;32(2):207–215, https://doi.org/10.1097/HJH.0b013e32836586f4.

14. Cheung N, Bluemke DA, Klein R, et al. Retinal arteriolar narrowing and left ventricular remodeling: the multi-ethnic study of atherosclerosis. *J Am Coll Cardiol*. 2007;50(1):48–55, https://doi.org/10.1016/j.jacc.2007.03.029.

15. Cheung N, Sharrett AR, Klein R, et al. Aortic distensibility and retinal arteriolar narrowing: the multi-ethnic study of atherosclerosis. *Hypertension*. 2007;50(4):617–622, https://doi.org/10.1161/HYPERTENSIONAHA.107.091926.

16. Wang JJ, Liew G, Klein R, et al. Retinal vessel diameter and cardiovascular mortality: pooled data analysis from two older populations. *Eur Heart J*. 2007;28(16):1984–1992, https://doi.org/10.1093/eurheartj/ehm221.

17. Wang J, Jiang J, Zhang Y, Qian YW, Zhang JF, Wang ZL. Retinal and choroidal vascular changes in coronary heart disease: an optical coherence tomography angiography study. *Biomed Opt Express*. 2019;10(4):1532–1544, https://doi.org/10.1364/BOE.10.001532.

18. Hwang TS, Gao SS, Liu L, et al. Automated quantification of capillary nonperfusion using optical coherence tomography angiography in diabetic retinopathy. *JAMA Ophthalmol*. 2016;134(4):367–373, https://doi.org/10.1001/jamaophthalmol.2015.5658.

19. Conrath J, Giorgi R, Raccah D, Ridings B. Foveal avascular zone in diabetic retinopathy: quantitative vs qualitative assessment. *Eye (Lond)*. 2005;19(3):322–326, https://doi.org/10.1038/sj.eye.6701456.

20. Tam J, Martin JA, Roorda A. Non-invasive visualization and analysis of parafoveal capillaries in humans. *Invest Ophthalmol Vis Sci*. 2010;51(3):1691–1698, https://doi.org/10.1167/iovs.09-4483.

21. Heagerty AM, Aalkjaer C, Bund SJ, Korsgaard N, Mulvany MJ. Small artery structure in hypertension. Dual processes of remodeling and growth. *Hypertension*. 1993;21(4):391–397, https://doi.org/10.1161/01.hyp.21.4.391.

22. Silva PS, Cavallerano JD, Sun JK, Soliman AZ, Aiello LM, Aiello LP. Peripheral lesions identified by mydriatic ultrawide field imaging: distribution and potential impact on diabetic retinopathy severity. *Ophthalmology*. 2013;120(12):2587–2595, https://doi.org/10.1016/j.ophtha.2013.05.004.

23. Hafner J, Pollreisz A, Egner B, Pablik E, Schmidt-Erfurth U. Presence of peripheral lesions and correlation to macular perfusion, oxygenation and neurodegeneration in early type II diabetic retinal disease. *Retina*. 2020;40(10):1964–1971, https://doi.org/10.1097/IAE.0000000000002704.

24. Tedeschi-Reiner E, Strozzi M, Skoric B, Reiner Z. Relation of atherosclerotic changes in retinal arteries to the extent of coronary artery disease. *Am J Cardiol*. 2005;96(8):1107–1109, https://doi.org/10.1016/j.amjcard.2005.05.070.

25. Hogan MJ, Feeney L. The ultrastructure of the retinal vessels. II. The small vessels. *J Ultrastruct Res*. 1963;49:29–46, https://doi.org/10.1016/s0022-5320(63)80034-9.